#3712

ON VALIDATION OF COMPUTATIONAL FLUID DYNAMICS: PROCEDURES FOR ROOM AIR MOTION PREDICTION

A.J. Baker, Ph.D., P.E. **R.M. Kelso, P.E.**

ABSTRACT

An ongoing ASHRAE research project seeks to identify and clarify key issues governing literate *application of computer-based analytical methods for prediction of room air motion. The engineering field is termed* "computational fluid dynamics," *with the acronym* "CFD," *which is maturing rapidly, paced by the incredible growth of scientific computing hardware capacity. As with any emerging technology, the production of* reliable predictions *requires a full understanding of intrinsic details. This paper addresses issues promoting literate use of CFD for prediction of room air fluid/thermal flow fields.*

INTRODUCTION

ASHRAE Research Project 464 seeks to quantify literate use of computational fluid dynamics (CFD) methodology for accurate prediction of room air motion flow fields and pollutant transport. The CFD requirement is attainment of accurate approximate solutions to the incompressible Reynolds-averaged Navier-Stokes equations, including a closure model for turbulence in room geometries.

Characterization of fluid/thermal incompressible flow classes is contained in nondimensional groupings, the most familiar of which is the ratio of inertia to viscous forces, termed the Reynolds number, $Re \equiv UL/\nu$. Here, U is a scale velocity, L is a characteristic room dimension, and ν is the fluid kinematic viscosity. For nonisothermal flows and the Boussinesq assumption regarding density body force effects, the ratio of inertia to buoyancy forces yields the nondimensional Grashof number, $Gr \equiv g\beta\Delta T L^3/\nu^2$. Here, g is the acceleration of gravity, β is the fluid compressibility, and ΔT is a scale temperature differential. The Prandtl number, $Pr = c_p\rho_o\nu/k$, also becomes introduced, where c_p is the specific heat, ρ_o is the reference density, and k is the fluid thermal conductivity.

Under actual room airflow conditions, representative orders of magnitude for these nondimensional groups are $Re \simeq 10^4 - 10^5$, $Gr \simeq 10^{11}$, and $Pr \simeq 10^0$. Since Re is well over the limit for which the flow field remains well ordered, i.e., laminar, the requirement exists to adjust the problem statement to account for "turbulence." The time-honored engineering approach is to statistically manipulate the governing mathematical description, hence introduce a "turbulent viscosity," ν^t, augmentation to diffusion effects. In distinction to the fluid kinematic viscosity, ν, the distribution of ν^t depends on the flow state, not the fluid present. Any such engineering model is an approximation of the true phenomena, hence the results of CFD analysis and experimental data will (must) exhibit some level of disagreement.

Therefore, the mathematical statement presented to a CFD algorithm/code designer is inaccurate to the extent that the true physics is modeled. This inherent difficulty is then compounded by the fact that any numerical simulation procedure can at best generate only an approximate solution to the established governing nonlinear partial differential equation (PDE) system. Further, while this PDE system is generally accepted as appropriate, additional approximations must be made to yield a computationally tractable statement. Specifically, no equation of state is available for incompressible flows, and the velocity field must always be divergence-free. Designing a CFD theory that accounts for these details introduces further approximations that can compromise prediction fidelity.

Finally, since a CFD numerical algorithm produces only an approximate solution to the terminal PDE system, numerical error mechanisms exist that further compromise prediction accuracy. Specifically, CFD methods operate on discretizations, termed the "computational mesh," upon which short wavelength solution information cannot be resolved. This introduces a dispersive error mechanism, producing mesh-scale solution oscillations if the discretization refinement is inadequate to resolve the CFD solution spatial gradients. Should these characteristic tell-tale oscillations fail to appear on coarse mesh computations, then irrefutable evidence thereby exists that the CFD solution is dominated by a numerical diffusion mechanism characterized by an artificial viscosity (ν^{art}). Without proper attention in the CFD algorithm/code design, ν^{art} effects can totally dominate those due to the physics model, ν^t, and the underlying kinematic effects in ν.

From this brief introduction, one can readily ascertain that reliable use of CFD methodology in room air motion prediction requires a literate user. The

A.J. Baker is a Professor in the Department of Engineering Science and Mechanics and **R.M. Kelso** is a Professor in the School of Architecture, University of Tennessee, Knoxville.

ASHRAE technical community must thus join with the aerospace community in its full recognition of the need for reliable "code validation." In the call for papers in a recent conference (AGARD 1988), code validation is defined as an effort to "ensure that the mathematical and numerical schemes employed in the code accurately model the critical physics of the flow field." The Ad Hoc Committee on CFD Validation of the Aeronautics Advisory Committee of NASA (Bradley 1988) has defined CFD code validation as "detailed surface-and-flow-field comparisons with experimental data to verify the code's ability to *accurately model* the *critical physics* of the flow. . . ."

Confidence in the predictions produced by a code thus accrues from investigating two issues:

1. Evaluation of the accuracy of the governing equations that are to be solved. These equations include assumptions due to using a simplified form of the Navier-Stokes equations or due to the modeling required for turbulent flow, transition, buoyancy, fluid-surface interaction, and other flow physics.
2. Determination of the accuracy of the numerical solution procedure for the chosen governing equations.

This paper addresses these issues for the room air motion problem class.

MATHEMATICAL STATEMENT

Since direct numerical simulation of turbulent flows is not tractable, even on today's supercomputers, a statistical manipulation is required to yield a computable form of the Navier-Stokes equation system for incompressible fluid/thermal flows. Several methods are appropriate, and the resultant rearrangement is termed the "Reynolds-averaged Navier-Stokes" equations. After a suitable nondimensionalization, this nonlinear partial differential equation (PDE) system governing unsteady turbulent incompressible fluid/thermal flow fields in vector form is

$$L(\rho_o) = \nabla \cdot u = 0 \tag{1}$$

$$L(u) = \frac{\partial u}{\partial t} + (u \cdot \nabla)u - \nabla \cdot \frac{1}{\mathrm{Re}}\left(1 + \nu^t\right)\nabla u + \nabla P - \frac{\mathrm{Gr}}{\mathrm{Re}^2}\Theta g = 0 \tag{2}$$

$$L(\Theta) = \frac{\partial \Theta}{\partial t} + (u \cdot \nabla)\Theta - \nabla \cdot \frac{1}{\mathrm{Re}}\left(\frac{1}{\mathrm{Pr}} + \frac{\nu^t}{\mathrm{Pr}^t}\right)\nabla\Theta - s_\Theta = 0 \tag{3}$$

$$L(C_A) = \frac{\partial C_A}{\partial t} + (u \cdot \nabla)C_A - \nabla \cdot \frac{1}{\mathrm{Re}}\left(\frac{1}{\mathrm{Sc}} + \frac{\nu^t}{\mathrm{Sc}^t}\right)\nabla C_A - s_A = 0 \tag{4}$$

The dimensionless parameters in Equations 2 through 4 are turbulent Prandtl number, turbulent Schmidt number, and the Grashof number with definitions,

$$\mathrm{Pr}^t = \frac{c_p \rho_o \nu^t}{k^t},\ \mathrm{Sc}^t = \frac{\nu^t}{D_{AB}^t},\ \mathrm{Gr} = \frac{g\beta(T_{max} - T)L^3}{\nu^2} \tag{5}$$

and the Reynolds number definition remains $\mathrm{Re} = UL/\nu$. The dependent variable set includes velocity vector, u, with scalar components u_i, $1 \le i \le n$, kinematic pressure ($P = p/\rho_o$), and potential temperature, Θ. In Equation 4, C_A is the mass or mole fraction of species A, and $\mathrm{Sc} \equiv \nu/D_{AB}$ defines the Schmidt number for binary diffusion. Finally, the Boussinesq buoyancy body force assumption is made in Equation 2, and g is the gravity unit vector.

The highest order spatial derivatives are present in Equations 2 through 4, hence each isolated equation is elliptic for finite Reynolds number, Re. Therefore, knowledge of fixed values of the dependent variables and/or their normal derivatives is required given everywhere on the boundary $\partial\Omega$ of the domain of definition $\Omega \subset R^n$, where n is the dimension of the problem statement. The generally admissible procedure is to specify velocity and temperature at a flow inlet to a region and to specify a heat flux on walls along with the no-slip velocity requirement. Neither velocity nor temperature may be specified at a location where the flow exits the region; the mathematically acceptable specification is that each variable leaves the domain with a vanishing normal derivative.

The system coupling via the continuity equation (Equation 1) creates a truly fundamental mathematical issue that forms the heart of any proposed CFD theory. Specifically, Equation 1 defines a differential constraint on velocity fields that are admissible as solutions to Equations 2 and 3. The requirement for a divergence-free field is intimately connected to the pressure (gradient) field that acts as a source term in Equation 2. However, neither an algebraic (i.e., equation of state) nor a differential equation is available for determination of pressure. Therefore, it must either be mathematically eliminated from Equation 2, via a dependent variable transformation to vorticity, or a computationally suitable procedure must be devised such that pressure becomes determinable from an iterative solution sequence. Any procedure for the latter must be compatible with knowledge regarding pressure on the domain boundary of Equation 2. The mathematically admissible situation is that static pressure may (must) be imposed at a flow outlet, and that the flow inlet pressure level will self-adjust such that a given inlet flow rate can be specified. No knowledge is available *a priori* regarding pressure distributions on nonflow through (wall) boundary segments.

In addition to these mathematical details, the PDE system (Equations 1 through 4) is not solvable since the turbulence eddy viscosity, ν^t, is not yet defined. A range of theoretical complexities exists for its modeling, each of which amounts to accumulation of many simplifying assumptions. For the room air problem class, the consensus appears that the two-equation turbulence kinetic energy (TKE) closure is the minimum acceptable, whereupon the definition for ν^t is

$$\nu^t \equiv C_\mu k^2/\epsilon \tag{6}$$

In Equation 6, k is the kinetic energy of the turbulent motion fluctuation about the mean flow, is the isotropic dissipation function describing the annihilation of turbulence energy into viscous heating, and C_μ is a correlation constant.

The PDE system governing k and ϵ is, in nondimensional form,

$$L(k) = \frac{\partial k}{\partial t} + \frac{\partial}{\partial x_j}\left(u_j k\right) - \frac{\partial}{\partial x_j}\left[\frac{1}{\mathrm{Re}}\left(1 + \frac{v^t}{\sigma_k}\right)\frac{\partial k}{\partial x_j}\right] - v^t \mathrm{Re}\frac{\partial u_i}{\partial x_j}\left(\frac{\partial u_i}{\partial x_j} + \frac{\partial u_j}{\partial x_i}\right) + \frac{1}{\mathrm{Re}}\epsilon + \frac{\mathrm{Gr}}{\mathrm{Re}}\frac{v_t}{\sigma_T}\nabla\Theta \cdot g = 0 \quad (7)$$

$$L(\epsilon) = \frac{\partial \epsilon}{\partial t} + \frac{\partial}{\partial x_j}\left(u_j \epsilon\right) - \frac{\partial}{\partial x_j}\left[\frac{1}{\mathrm{Re}}\left(1 + \frac{v^t}{\sigma_\epsilon}\right)\frac{\partial \epsilon}{\partial x_j}\right] - C_1 f_1 v^t \mathrm{Re}\left[\frac{\partial u_i}{\partial x_j}\left(\frac{\partial u_i}{\partial x_j} + \frac{\partial u_j}{\partial x_i}\right)\right] + C_2 f_2 \frac{1}{\mathrm{Re}}\frac{\epsilon^2}{k} + C_3 \frac{\mathrm{Gr}}{\mathrm{Re}}\frac{v^t}{\sigma_T}\frac{\epsilon}{k}\nabla\Theta \cdot g = 0 \quad (8)$$

Equations 7 and 8 are written in tensor index notation with summation over the spatial dimensionality n when repeated in any term. This (tensor) precision is required to correctly define the turbulence production terms involving $\partial u_i/\partial x_j$, which tightly connect Equations 7 and 8 to Equations 1 through 4. The variable and parameter definitions remain customary, and a wide range of correlation model constants and functions are required to close Equations 7 and 8. For example, the Lam-Bremhorst model (Lam and Bremhorst 1981) specifies

$$\begin{aligned} f_1 &= 1 + (0.05/f_\mu)^3 \\ f_2 &= 1 - \exp(-R_T^2) \\ f_\mu &= [1 - \exp(-0.0165R_y)]^2(1 + 20.5/R_T) \\ C_\mu &= 0.09 \\ C_1 &= 1.44 \\ C_2 &= 1.92 \\ C_3 &= 0.4 \text{ to } 1.44 \text{ (function of flux Richardson number } R_T) \\ \sigma_k &= 1.0 \\ \sigma_\epsilon &= 1.3 \\ \sigma_T &= 0.9 \\ R_T &= k^2/v\epsilon \\ R_y &= \sqrt{ky}/v \text{ where } y = \text{normal distance from wall} \end{aligned} \quad (9)$$

The issue of boundary conditions for Equations 7 and 8 raises a serious computational complication. The dominant spatial derivations are again second order, hence Equations 7 and 8 are each (isolated) elliptic boundary value problems. The mathematically exact wall boundary conditions are $k = 0$ and $\partial\epsilon/\partial n = 0$, where n is the normal direction to the wall. However, as thoroughly documented in the literature (Patel et al. 1985), very large spatial gradients in both k and ϵ exist in regions directly adjacent to solid walls. The computational mesh refinement required to adequately resolve these distributions places a very severe burden on computer resources, hence essentially *all* code implementations utilize "wall function" relationships instead. These are derived from boundary layer similarity considerations and yield replacement boundary condition expressions applied at an appropriate distance from the actual wall surface.

The use of such wall functions is accurate for attached boundary layer flows only; their use is a significant compromise for general omnidirectional flows with recirculation regions. Figure 1 illustrates the savings that accrue to use of wall functions for an isothermal boundary layer flow. The graph symbols denote node points of the wall-normal mesh. Note that the wall-function-predicted boundary layer velocity decreases to only about 70% of freestream (Figure 1a), while the true value is zero (Figure 1b). Similar distinctions are present in the k and ϵ comparisons as well.

The complete governing PDE system for room air motion flow prediction is established in Equations 1 through 8. It is extremely nonlinear and any CFD theory derived to seek an approximate solution is significantly challenged by attendant intrinsic numerical error mechanisms. The dominant error mode is short wavelength dispersion yielding local solution oscillations. In the absence of an adequate mesh to resolve solution spatial gradients, the "universal" correction for practically all CFD codes is to augment the genuine laminar and turbulent diffusion mechanisms with a numerical diffusion operator that dissipates these discretization-created oscillations. Unless great care is taken in the CFD formulation, the net effect is to modify the dissipation term multiplier in Equation 2 to the form

$$\frac{1}{\mathrm{Re}}\left(1 + v^t\right) \Rightarrow \frac{1}{\mathrm{Re}}\left(1 + v^t + v^{art}\right) \quad (10)$$

The coefficient of artificial viscosity, v^{art}, is either a function of integration time step, Δt, or a characteristic length scale, h, of the local mesh. The larger either Δt or h is, the more significant v^{art} becomes in comparison to v^t and/or laminar viscosity (the 1/Re term) effects. Therefore, this error mechanism can only be controlled by use of small time steps and/or an adequate mesh so that Δt and/or h is kept sufficiently small. Without these constraints, and on coarse computational meshes, the CFD algorithm prediction will become totally dominated by v^{art}, yielding smooth-appearing computational trash. The issue of advanced turbulence closure modeling then truly becomes moot. The "literate" user of CFD simulation packages must be fully cognizant of these issues.

BASIC PRECEPTS OF CFD ALGORITHMS

The first requirement of a CFD algorithm/code design is to rearrange the established governing PDE system (Equations 1 through 9) into a mathematically well-posed statement. What distinguishes such a "conservation law system (CLS)" from a PDE system is establishment of initial and boundary conditions for

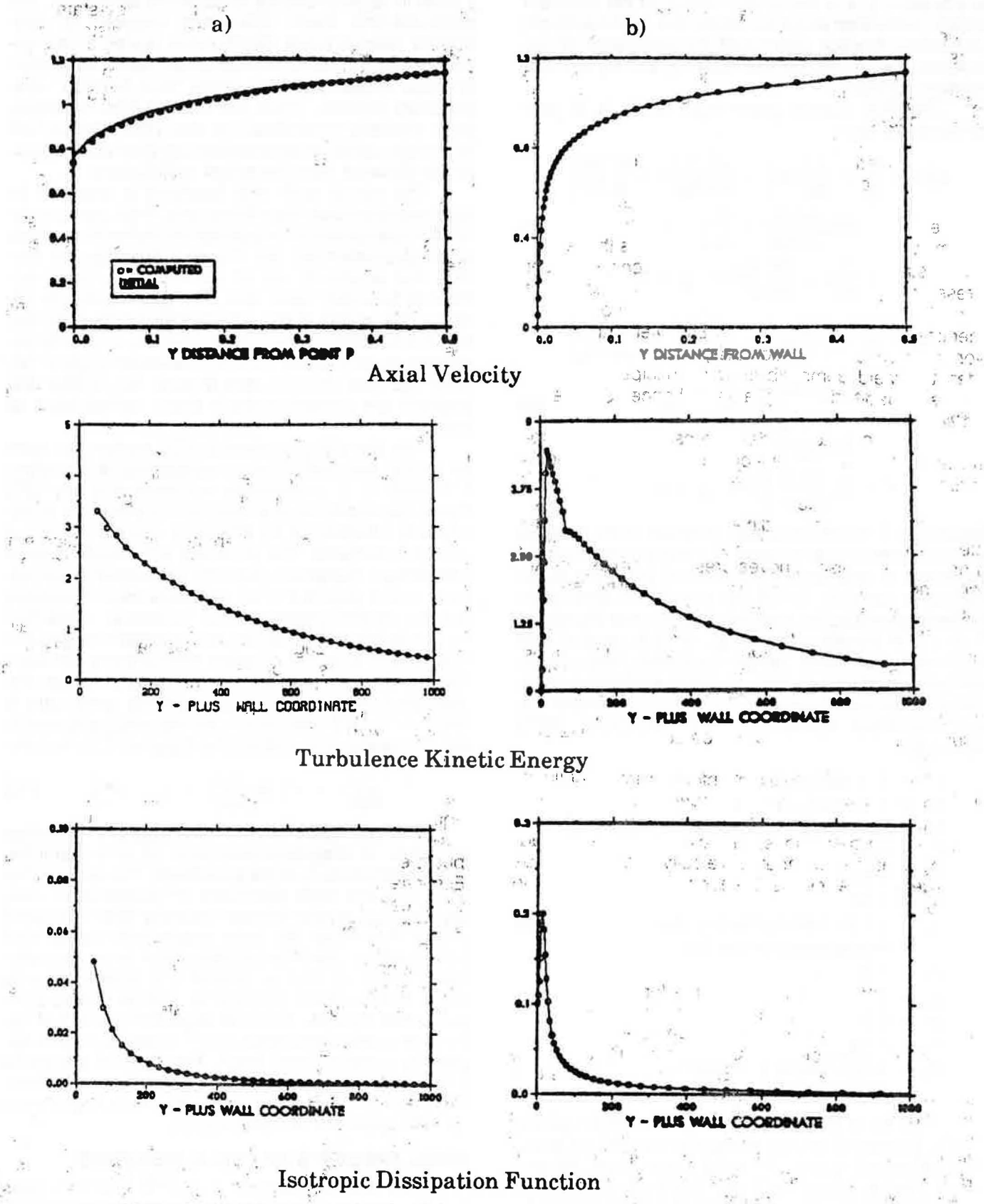

Figure 1 *Comparison of wall function and exact TKE closure boundary conditions, attached fully developed turbulent flow, Re = 41,667; a) wall function U, K, and E; b) exact boundary condition U, K, and E*

which one can mathematically guarantee that a solution exists and that in fact it is bounded by what one puts in as initial and boundary conditions.

The mathematical interconnection between the continuity equation (Equation 1) constraint of velocity divergence-freeness and pressure is the critical issue, and two fundamentally distinct CLS resolutions exist. The mathematically exact enforcement of Equation 1 requires use of vector field theory, since the curl of a vector potential always possesses vanishing divergence. Hence u can be replaced by $\nabla \times \Psi$, and the n-dimensional stream vector, Ψ, becomes the familiar scalar stream function Ψ in two dimensions. However, pressure is still present in Equation 2 with no resolution. Since the curl of a scalar gradient also vanishes identically, forming the curl of $L(u)$ yields the vector vorticity transport equation $L(\Omega)$. Finally, these vector identities yield compatibility relationships among the derived dependent variables, hence closure is achieved.

Two fundamental detractions exist to this formulation. In three dimensions, the Ω-Ψ compatibility equation does not yield a well-posed CLS unless Ψ is also divergence free. This occurs intrinsically in two dimensions, but in three dimensions it will not generally be achievable. Alternatively, the vorticity-velocity transformation also removes pressure from explicit appearance, and the resultant compatibility relations yield a well-posed CLS in n dimensions since $\nabla \cdot u = 0$ identically. The vorticity PDE system is elliptic in either instance; hence, vorticity and/or its normal derivative needs to be known all around the boundary. This information unfortunately depends upon the state of flow in the boundary region and is not known *a priori;* thus it must be computed, which constitutes the second detraction.

The alternative to exact enforcement of continuity is to develop an inexact procedure, and several have been proposed over the years, each with its individual features and detractions. One class is formed by admitting that any computed velocity field will not be divergence free; hence Equation 1 can be written in the form

$$L(\rho_o) = \nabla \cdot u + \frac{\partial q}{\partial t} = 0 \qquad (11)$$

If the time derivative of the source function q can be driven to zero, then Equation 11 reverts to Equation 1 and the continuity constraint becomes enforced.

The time-explicit MAC algorithm (Roach 1972) was the first developed for Equation 11, with the definition $q \equiv \nabla \cdot u^h$, where superscript h denotes use of a computational mesh, Ω^h. The original derivation used the symbol "D" for q, and at steady state $\partial D/\partial t = 0$ and indeed Equation 11 coincides with Equation 1. Murakami et al. (1987) employ the MAC algorithm in their room air motion simulation flow code.

A time-implicit successor to the MAC algorithm was formulated (Chorin 1967) for the definition $q \equiv p/\beta$, where β is a fictitious compressibility coefficient and p is pressure. Hence, Equation 11 becomes an initial-value problem statement for pressure. For a suitable resolution of boundary values, the steady-state solution yields $\partial p/\partial t = 0$, i.e., the pressure distribution is stationary. No application of this pseudo-compressibility formulation is reported for the room air motion problem class. However, Kwak et al. (1986) developed such a code for isothermal incompressible aerodynamics applications.

Another class of inexact formulations is based on the hypothesis that a correction procedure applied to a nondivergence-free velocity field can be formulated into a pressure correction. Spalding and his students, as summarized in Patankar (1980), originated the "SIMPLE" pressure correction algorithm requiring solution of a Poisson equation. There have been many commercial code implementations of this algorithm, and many individual researchers have programmed their own codes for room air motion analyses (Haghighat et al. 1989). This theory is viable only for steady-state flow prediction, and convergence is said to occur (typically) when the maximum local error in discrete satisfaction of Equation 1 is nominally 1%. Recently, Noronha and Baker (1989) have formulated the more exact theory and have extended its applicability to time-accurate solution of unsteady problem statements.

Still another class of an inexact formulation employs a penalty constraint theory, which algebraically equates the pressure field to the error in velocity field divergence-freeness through a constant of the order $(Re)^{-1}$ (Baker 1983, chapter 5). One commercially available code (Engleman 1984) is based on this CFD theory, which is applicable to both unsteady and steady-state flow prediction. No applications of this code or theory are reported in the room air literature, although wide use is reported for thermal/fluid analysis.

The preceding paragraphs highlight the first decision required by a CFD algorithm designer. An equally fundamental decision regards the design decisions required to convert the derived CLS into a computable form, i.e., a set of algebraic equations. Essentially all incompressible flow CFD numerical theories can be analyzed as decisions made in constructing an approximation to a weak statement written on the governing CLS. This system is constituted of Equations 1 through 4 and Equations 7 and 8 and their various rearrangements, each of which is an initial-value, elliptic boundary value statement of the form

$$L(q) = \frac{\partial q}{\partial t} + \frac{\partial}{\partial x_j}(f_j - f_j^v) - s = 0, \text{ on } \Omega \subset R^n \qquad (12)$$

As presented in Baker (1983), $q(x,t)$ is the generalized dependent variable (array) and f_j is the kinematic/kinetic flux vector containing the fluid convection terms $(u \cdot \nabla)q$ and pressure. Further, f_j^v is the dissipative flux vector containing the 1/Re and turbulence closure model terms, s is the source term peculiar to each individual PDE, and Ω is the domain of definition of $L(q)$ of dimensionality n. In addition to Equation 12, well-posed CLS manipulations can yield a Poisson equation coupled with Equation 12. The form is

$$L(q^*) = -\frac{\partial^2 q^*}{\partial x_j^2} - s(q) = 0 \qquad (13)$$

where the source $s(q)$ is a function of select variables in q satisfying Equation 12.

A CFD algorithm is thus required to transform the solution of the nonlinear conservation law system (Equations 12 and 13), with determined appropriate boundary conditions, into a computable form. The generalized weak statement theory (Baker and Pepper 1990) defines an algorithm as a semi-discrete approximation to a weak statement (WS) written on $L(q)$ and $L(q^*)$,

$$WS \equiv \int_\Omega w\, L(q)d\tau \equiv 0, \text{ for all } w(x) \qquad (14)$$

where the set of weight functions $W(x_j)$ is completely arbitrary. Specifically, if one chooses that w is the set of all constants, then Equation 14 expresses the constraint statement underlying "finite difference" and/or "finite volume" CFD algorithms, of which the cited MAC, pseudo-compressibility, and SIMPLE theory implementations are examples. Conversely, if the set w is allowed to be functions of x_j, then an entire class of "finite element" algorithms is established, e.g., the referenced penalty method.

Equation 14 is not a computable form since the state variable q remains unknown. One must thus seek an approximation for $q(x_j,t)$, and any approximation can be expressed as an expansion into the product of the N known functions $\Psi_i(x_j)$ and the N unknown expansion coefficients Q_i as

$$q^N(x_j,t) \equiv \sum_{i=1}^{N} \Psi_i(x_j)Q_i(t) \qquad (15)$$

The corresponding approximation to any weight function $w(x_j)$ is

$$w^N(x_j) \equiv \sum_{i=1}^{N} \Phi_i(x_j)W_i \qquad (16)$$

where the function set Φ_i may certainly be distinct from Ψ_i in Equation 15. The theoretical preference, termed "Galerkin," is that the weight set, Φ_i, indeed be identical to the function set, Ψ_i, employed to support the semi-discrete approximation. In any case, the W_i in Equation 16 are *known* expansion coefficients of the interpolant $w^N(x_j)$ of the specified test function $w(x_j)$.

Note that Equations 14 through 16 are equally valid for approximating any Poisson variable q^*, which is implicitly time-dependent through $s(q)$. This being the case, the distinguishing notation can now be deleted. The approximation function sets $\Psi_i(x_j)$ and $\Phi_i(x_j)$ are chosen by the CFD algorithm designer, either explicitly or by default, from a very small subspace of functions in H^m, the Sobolev space containing all functions with m^{th} order spatial derivatives that are square integrable. Since algorithm designers also choose to discretize the solution domain with a computational mesh Ω^h, a "compact support" CFD algorithm results for choosing Ψ_i as the local set of (Lagrange) interpolation polynomials with knots at the mesh nodal coordinates.

For the choice of using a discretization Ω^h, the resultant dominant approximation error mechanism is a phase dispersion that can induce shortwave oscillations. Following a generalized analysis (Baker and Kim 1987), a semi-discrete temporal Taylor series constructed on Equation 12 yields a companion CLS amenable to exacting analysis for control of this error mechanism. The resultant modified form for Equation 12 is

$$L^m(q) = \frac{\partial q}{\partial t} + \frac{\partial}{\partial x_j}(f_j - f_j^\nu) - s - \frac{h\partial}{|u|\partial x_j}\left(\alpha A_j \frac{\partial q}{\partial t} + \beta A_j A_k \frac{\partial q}{\partial x_k}\right) + \ldots \qquad (17)$$

where the matrix $A_j = \partial f_j/\partial q$ is the Jacobian of the kinematic flux vector f_j in Equation 12, $|u|$ is velocity magnitude, h is a length scale, and α and β are coefficients eligible for optimization.

Since Equation 13 contains no time derivative, an operation similar to Equation 17 is not appropriate for the Poisson variable (if present). Hence, without loss of clarity, the Taylor weak statement (TWS) CFD theory for Equations 12 and 13 for any semi-discrete approximation (Equations 15 and 16) is

$$TWS^N = \int_{\Omega^h} w^N(x)L^m(q^N)d\tau = 0, \text{ for all } w^N(x) \qquad (18)$$

The complete arbitrariness required for $w^N(x_j)$ in Equation 14 can now be accounted for analytically by determining the extremum of Equation 18 with respect to the known expansion coefficients W_i in Equation 16. Using the standard Taylor series concept, the stationary point of Equation 18 for all possible choices for W_i, for $1 \le i \le N$, is

$$\frac{\partial(TWS^N)}{\partial W_i} \equiv \{0\} = \int_\Omega \Phi_i(x)L_m(q_N)d\tau, \text{ for } 1 \le i \le N \qquad (19)$$

Since the functions $\Phi_i(x)$ are all known, as are the solution approximation functions, $\Psi_i(x)$, all integrals expressed in Equation 19 are theoretically evaluable. Therefore, realizing that time t remains a continuous variable, Equation 19 for CLS (Equation 17) yields an ordinary differential equation (ODE) system

$$\partial TWS^N = [M]\frac{d\{Q\}}{\partial t} + \{R\} = \{0\} \qquad (20)$$

Correspondingly, for the Poisson PDE (Equation 13), if present, Equation 19 produces the algebraic system

$$\partial TWS^N = \{F(Q)\} = [D]\{Q\} - \{S\} = \{0\} \qquad (21)$$

In Equations 20 and 21, the bracket notation $[\cdot]$ signifies an order N square matrix and the brace $\{\cdot\}$ denotes the corresponding order column matrix.

Since a CFD algorithm must transform a PDE system into a completely algebraic statement, a temporal discretization step is required for Equation 20.

Both explicit and implicit formulations are usable, and the generic single-step ODE algorithm family amounts to evaluation of the discrete Taylor series

$$\{Q\}^{n+1} = \{Q\}^n + \Delta t\left(\theta \frac{d\{Q\}^{n+1}}{dt} + (1 - \theta)\frac{d\{Q\}^n}{dt}\right) \tag{22}$$

for any $0 \leq \theta \leq 1$. The ODE matrix system (Equation 20) expresses the time derivative needed to complete Equation 22, hence one directly obtains the terminal algebraic system

$$\{F(Q)\} = [M]\{Q^{n+1} - Q^n\} + \Delta t\left(\theta\{R\}^{n+1} + (1 - \theta)\{R\}^n\right) = \{0\} \tag{23}$$

The established CFD algorithm statements, Equations 22 and 23, are fully algebraic, and both are expressed in the homogeneous form $\{F(\cdot)\} = \{0\}$. This is particularly convenient for direct insertion into a generic (Newton) matrix iteration algorithm, from which any numerical linear algebra computational procedure can be developed. The basic Newton statement is

$$[J]_p\{\delta Q\}_{p+1} = -\left([M]\{\Delta Q\}_p^{n+1} + \Delta t(\theta\{R\}_p^{n+1} + (1 - \theta)\{R\}^n)\right) \equiv -\{F(Q)\} \tag{24}$$

where $[J] \equiv \partial\{F\}/\partial\{Q\}^{n+1}$ is the Newton Jacobian, p is the iteration index, and n and $n + 1$ refer to the appropriate time levels t^n and t^{n+1}. The resultant CFD nodal solution is given by

$$\{Q\}^{n+1} = \{Q\}^n + \{\Delta Q\}^{n+1} \tag{25}$$

$$\{\Delta Q\}^{n+1} = \sum_p \{\delta Q\}_{p+1}, \text{ for } p \geq 0 \tag{26}$$

ROOM GEOMETRY BENCHMARK EXPERIMENTS

Overview

Code validation is a fundamental prerequisite to use of CFD methodology for room air motion prediction. As stated, validation includes verified ability to accurately model—hence capture—the correct physics of a given problem. This implies an adequate closure model for turbulence, etc., and an adequate discrete analog for the resultant governing equation system. Realizing that any turbulence closure, e.g., TKE, is at best a model, then disparity is always expected between experiment and prediction for complicated, non-boundary-layer turbulent flows. Conversely, several quality laminar flow benchmark problems exist that are highly demanding for characteristic physics, hence control of strictly numerical error mechanisms in a CFD algorithm.

Emphasis is appropriate on the latter, since if one can guarantee control of the numerical error mechanisms, then, in the progression to turbulent flow simulation, the only error mechanism remaining must reside in the closure model. A further substantiation for this approach stems from recognition that the dominant dispersive CFD numerical error mechanism manifests mesh-scale oscillations when the mesh is inadequate for resolving the local solution gradients. Diffusion mechanisms moderate this oscillating error mode and, recalling Equation 10, the effective diffusion mechanism present in a CFD algorithm is

$$D_{eff} = \frac{1}{\mathrm{Re}}\left(1 + \nu^t + \nu^{art}\right) \tag{27}$$

Certainly, control of ν^{art} is critical to the validation requirements for ν^t.

It is important to determine the range for D_{eff} that is appropriate for room air motion turbulent simulations. Recall that $\mathrm{Re} = UL/\nu$ is the classic Reynolds number. In a room geometry, a typical dimension is $L \approx 10$ ft and a representative velocity scale may be $U \approx 120$ ft/m. The room-temperature kinematic viscosity of air is $\nu \approx 1.6 \times 10^{-4}$ ft^2/s; hence, in consistent units,

$$\mathrm{Re} = \frac{UL}{\nu} \approx \frac{2 \cdot 10}{1.6 \times 10^{-4}} \approx 10^5 \tag{28}$$

For fully turbulent flow, a representative turbulent/laminar viscosity ratio is the order $\nu^t/\nu \leq 10^2$. Thus, Equation 27 becomes

$$D_{eff} = \frac{1}{\mathrm{Re}}\left(1 + \nu^t + \nu^{art}\right) \approx 10^{-5}\left(1 + 10^2 + \nu^{art}\right) \approx 10^{-3} \tag{29}$$

if ν^{art} is controlled. Hence, the "effective Reynolds number (Re*f*)" of a representative turbulent flow CFD simulation is about $\mathrm{Re}f \cong 10^3$.

The nondimensionalization of the Navier-Stokes equations for laminar natural convection employs a representative velocity, U, scaled on the thermodynamic variables. This produces a unit Reynolds number ($\mathrm{Re} = 1$) identically, and introduces the Rayleigh number, $\mathrm{Ra} = \mathrm{Gr}/\mathrm{Re}^2 = \mathrm{Gr}$, where Gr is the Grashof number. Thus,

$$\mathrm{Ra} = \frac{g\beta\Delta T L_i^3}{\nu^2} \tag{30}$$

and for unit temperature difference ΔT and unit length scale L, $\mathrm{Ra} \approx 10^7$ for air, while a decade increase in both yields $\mathrm{Ra} \approx 10^{11}$. In the event that the natural convection flow is turbulent, then for $\nu^t/\nu \approx 10^2$, the CFD "effective Rayleigh number (Ra*f*)" range becomes $10^3 \leq \mathrm{Ra}f \leq 10^7$.

This briefly illustrates establishing a set of effective parameters pertinent to CFD simulation of turbulent room air motion flow. The concepts of "Re*f*" and "Ra*f*" allow one to efficiently conduct CFD benchmark experiments in the absence of a turbulence closure model that invariably increases code computing costs by an order of magnitude or more.

Natural Convection in a Square Cavity

This thermal problem statement is the fundamental natural convection benchmark for the room air motion class. It is constituted of a square room (do-

main) with opposed fixed temperature vertical surfaces and adiabatic top and bottom surfaces (see Figure 2a). The flow is viscous, hence the velocity vector vanishes all around the boundary. A representative uniform computational mesh containing 17 × 17 node points is shown in Figure 2b. Figures 2c, 2e, and 2g graph the computed steady-state velocity vector fields for $10^3 \leq Raf \leq 10^5$ as obtained using the CFD lab vorticity-stream function TWS pilot code (Woods 1989). The corresponding temperature distributions are shown in both a surface perspective and as planar isotherm contours in Figures 2d, 2f, and 2h. The former presentation highlights the temperature gradients resolved, hence the related heat flux distributions to the walls.

The first question to pose of any given CFD experimental data set is, "Is the mesh adequate to resolve the solutions features, and are these data accurate?" Provided the CFD algorithm can absolutely control v^{art}, one can assess mesh adequacy by viewing solution smoothness, since oscillations will occur in the solution if the mesh is inadequate. In the vorticity-stream function formulation, velocity is determined from vorticity, the computational primitive most susceptible to dispersion error. The perspective vorticity solution surface provides the observation venue, and Figures 3a through 3f summarize the benchmark test results on two computational meshes. For $10^3 \leq Raf \leq 10^5$, the 17^2 uniform mesh solution is free of short-wave oscillations (Figures 3a through 3c), hence the mesh appears adequate. However, for $Raf = 10^6$, the solution near the walls exhibits an oscillation (Figure 3d). In the absence of artificial viscosity, the 17^2 uniform mesh is verified definitely inadequate for $Raf \geq 10^6$.

Two acceptable approaches are available to resolve the issue of mesh inadequacy. The best procedure is to increase the uniform mesh density, which considerably increases computer CPU cost. Figure 3e presents the steady-state solution for $Raf = 10^5$ obtained on the double-density uniform 33^2 mesh. The 17^2 and 33^2 solutions are quite comparable, although added local detail in the latter is certainly evident.

The next best procedure is to rearrange the given mesh to nonuniform, to move more resolution into the high-gradient regions. Comparing Figures 3d and 3f confirms that a nonuniform 17^2 mesh, with added wall resolution somewhat resolves the oscillations at $Raf = 10^6$. However, since the domain middle region now has even less resolution, associated solution detail is lost. An unacceptable approach is to add artificial viscosity v^{art} to the CFD algorithm. This approach simply augments the effective diffusive processes; hence the computer printed output for Raf does not correspond to physical reality.

An important accuracy comparison for this benchmark room air problem is the distribution of wall heat flux. The Nusselt number, Nu, is the appropriate variable, and Figure 4 graphs the computed range and average value of Nu vs. Raf. The comparison to available experimental and computational data is excellent over the range of Raf evaluated. Note that Nu varies two orders of magnitude about the average at $Raf = 10^6$.

Isothermal Step Wall Diffuser

Most room geometries involve ventilation introduction via an inlet of small characteristic dimension in comparison to a room dimension. The benchmark problem for which quality experimental data exist is the isothermal step wall diffuser. As sketched in two and three dimensions (Figures 5a and b), flow enters from the left in a duct of characteristic width h into a chamber of characteristic dimension $H > h$. The onset flow first separates at the step, then eventually reattaches, yielding one or more closed recirculation regions. The axial extent, intercept, and number of these recirculation zones is directly dependent on Reynolds number, Re. Armaly et al. (1983) report experimental results for $H \approx 2h$ in the three-dimensional geometry of Figure 5b, which is summarized in Figure 5c as the loci of the primary, secondary, and tertiary recirculation region separation and reattachment coordinates (defined in the inset sketch). The flow field remains two-dimensional and laminar to $Re \approx 800$, then becomes fully three-dimensional prior to onset of turbulent flow at $Re \approx 3000$. The turbulence becomes fully developed by $Re \approx 6500$, hence the flow field returns to two-dimensionality for $Re > 6500$. Note in Figure 5c that the primary recirculation region extent is identical at $Re \approx 300$ and $Re \geq 7000$, adding credence to the concept of Ref as well as the nominal 10^2 factor for eddy viscosity ratio (Equation 29).

Noronha and Baker (1989) report comparisons among TWS vorticity-stream function and velocity-penalty algorithms and this experiment. Figure 6a summarizes the steady-state laminar velocity vector fields obtained for the nondissipative ($v_\omega = 0$) ω-Ψ algorithm for $10 \leq Ref \leq 2000$. The comparison data obtained by the TWS penalty algorithm (Figure 6b) degrade significantly by $Ref = 400$, whereupon the dispersive error mode begins to dominate. In the range for which the experiment remains two-dimensional, the TWS prediction of primary recirculation region span is in excellent agreement with the experiment (Figure 6c). Finally, note that the vorticity algorithm predicts progressively more recirculation regions as Ref increases to 2000, in qualitative agreement with the experiment (Figure 5c), which, however, has transitioned to a fully three-dimensional flow field.

Pollutant Transport

The accurate CFD prediction of transport of a scalar inert species via numerical solution of Equation 4 is also challenging. Two benchmark test case specifications are available for definitive comparison with computed solutions. The first is purely convective, while the second mixes convection and uniform but directional diffusion, and either can be cast in two- or three-dimensional form.

One benchmark is familiarly termed the "rotating cone" and constitutes pure convection of a scalar, point-symmetric initial distribution by a solid body rotation velocity field. Hence, in Equation 4, $u = ui +$

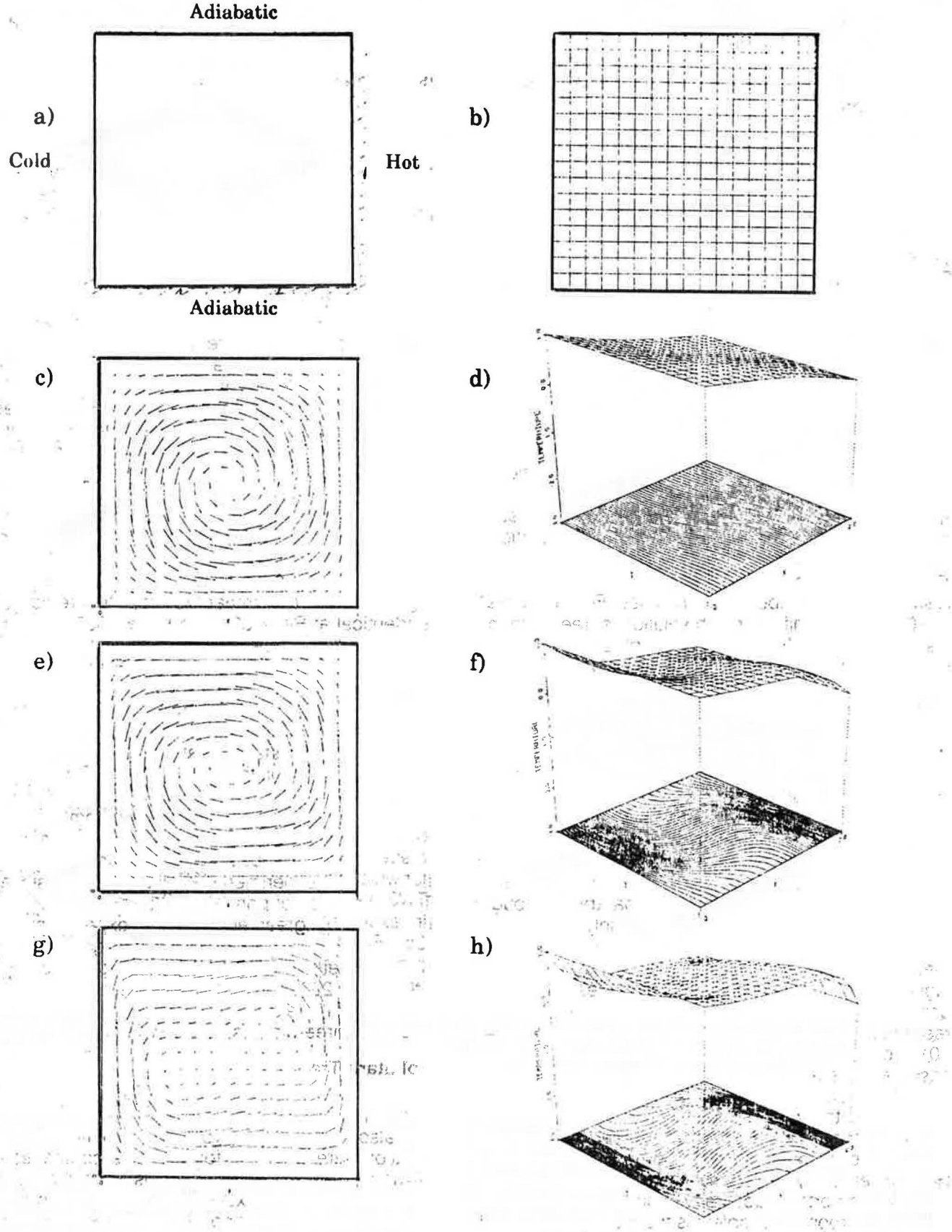

Figure 2 *Natural convection square cavity benchmark, TWS vorticity-stream function algorithm, steady state; a) geometry; b) 17² uniform mesh; c) Raf = 10³, velocity; d) temperature; e) Raf = 10⁴, velocity; f) temperature; g) Raf = 10⁵, velocity; h) temperature*

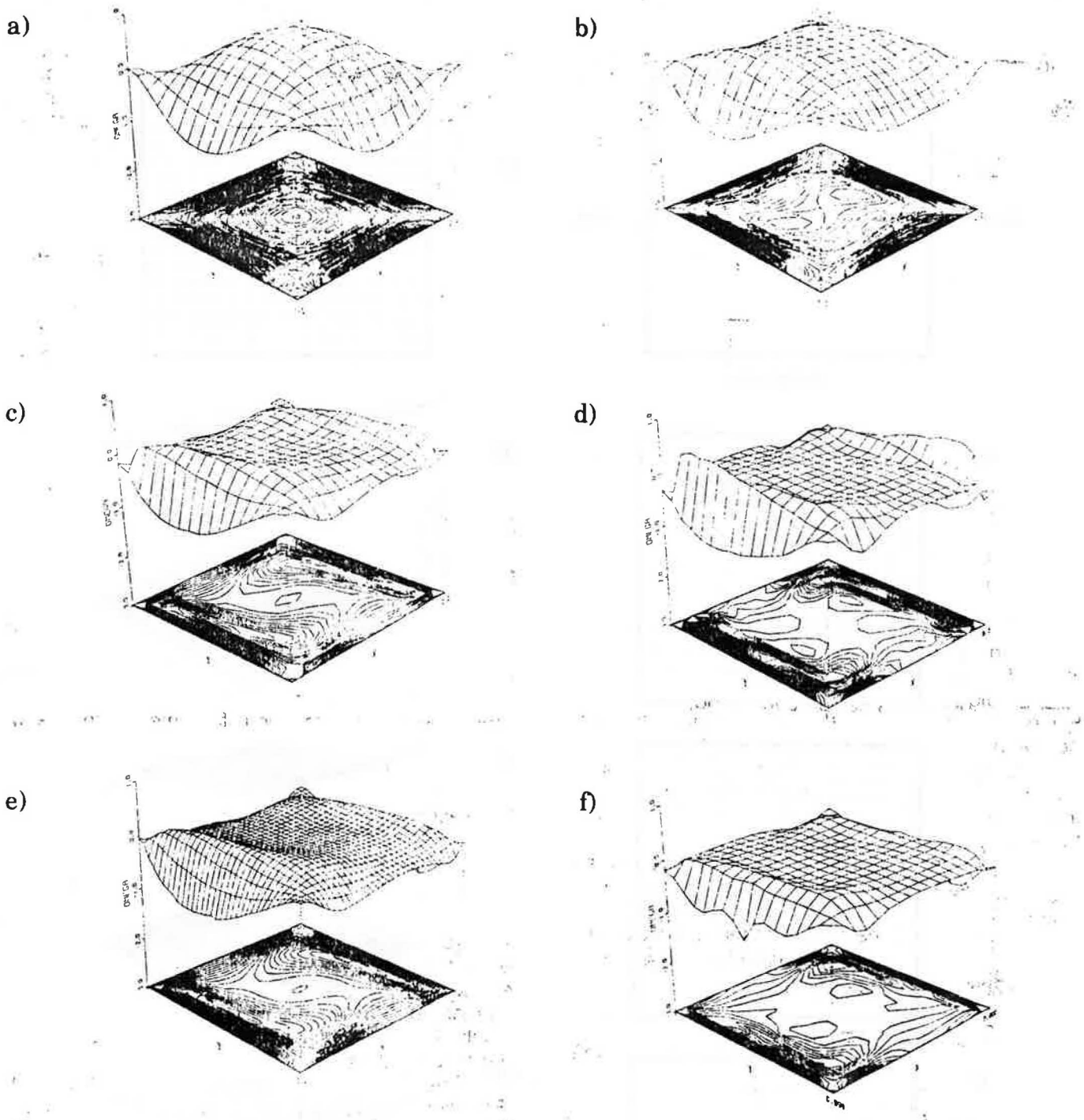

Figure 3 *Natural convection square cavity benchmark, TWS vorticity-stream function algorithm, steady-state vorticity distribution; a) uniform 17^2 mesh, Raf = 10^3; b) Raf = 10^4; c) Raf = 10^5; d) Raf = 10^6; e) uniform 33^2 mesh, Raf = 10^5; f) non-uniform 17^2 mesh, Raf = 10^6*

$vj = r\theta e_\theta$ is the input velocity field in two dimensions, while in three dimensions $u = ui + vj + wk = r\theta e_\theta + wk$. In both cases, e_θ is the unit vector parallel to the locus r = constant and θ is angular velocity. In three dimensions, w greater or less than zero translates the planar profiles parallel to the z axis.

Baker (1983) compares various CFD algorithm performance for this problem for the case where $C_A(z = 0)$ is an axisymmetric, rotated cosine distribution. Figure 7a illustrates this initial distribution in perspective view, and also shows the sense of imposed convective motion. The problem possesses no steady state, and the exact solution is pure rotation of the initial condition without distortion. Figures 7b through e illustrate computed results obtained for various CFD algorithms following what should be one complete revolution of the initial condition. An implicit quadratic basis finite-element Galerkin algorithm using a non-dimensional time step of 0.25 produces the most accurate solution (Figure 7b). Increasing this time step

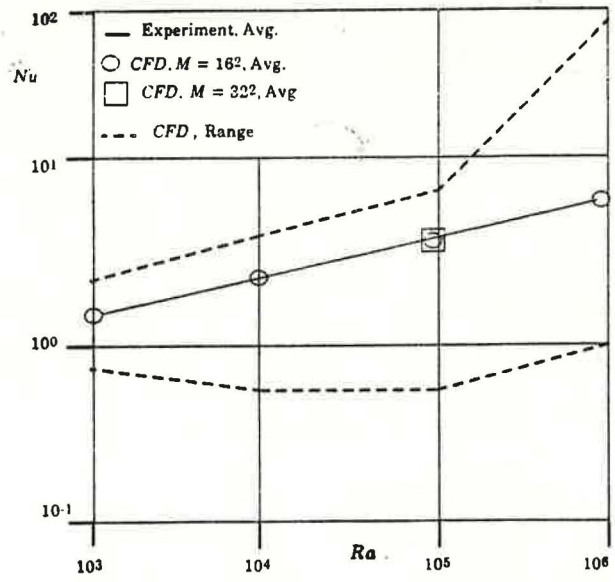

Figure 4 *Nusselt number comparison, CFD to available data, natural convection thermal cavity*

to 0.5 decreases accuracy (Figure 7c), hence the inherent underlying dispersive error mode is more visible in the background plane. The linear basis finite-element algorithm is easier to form and, as evident in Figure 7d, produces a relatively larger magnitude dispersive oscillation, as documented by the elevation of the plot base. Finally, Figure 7e shows the Crank-Nicolson finite difference algorithm solution obtained at the same integration time step, which is highly distorted by phase dispersion error.

The second convection with diffusion benchmark corresponds to a continuous source emission into a unidirectional imposed flow field with diffusion processes non-zero in the plane normal to this velocity. The exact solution to this "Gaussian plume" specification (Baker 1983, p. 213) is

$$C_A(x_i) = \frac{S}{2\Pi\sigma_y\sigma_z U} e^{-y^2/2\sigma_y^2} \left(e^{-(H-z)^2/2\sigma_z^2} + e^{-(H+z)^2/2\sigma_z^2} \right) \qquad (31)$$

where C_A = pollutant concentration at point x, y, z; S = emission rate of the source; u = average wind speed ($U_0 = ui$); x = downwind distance from source; y = crosswind distance measured from plume centerline; z = elevation above ground level; H = elevation of the source above ground level; σ_y = horizontal diffusion coefficient; and σ_z = vertical diffusion coefficient. Figure 8 compares finite-element Galerkin algorithm computed steady-state distributions to Equation 31, denoted therein as "Gaussian," for the case of a pyramidal source with $S = 100 g/m^2 s$, $u = 1$ m/s, $\sigma_y = 0.1 m^2/s$, and $\sigma_z = 0.5$ m^2/s for the three-dimensional case. Simulations were conducted using the linear and the quadratic basis algorithm formulation, and the data presentations compare symmetric half-plane CFD results with the analytical centerline results and analytical lateral spread at the outflow plane. Again, the quadratic basis algorithm results are uniformly more accurate; in comparison, the linear basis centerline trajectory is underpredicted by approximately one nodal span length.

Turbulent Boundary Layer

In many instances following air introduction into a room, the resultant flow field approximates a developing boundary layer up to encountering an obstacle or a corner. An excellent comparison base to validate wall function and/or low Reynolds number CFD implementations for a TKE model exists in Cole's law, an empirically derived correlation of a wealth of turbulent boundary layer experimental data. The correlation, expressed in nondimensional form where $u^+ = u/U_r$, is

$$u^+ = \frac{1}{K} \ln y^+ + B + \frac{2\Pi}{K} \sin^2\left(\frac{\Pi y}{2\delta}\right) \qquad (32)$$

In Equation 32, $K = 0.4$ is Karmann's constant, $B = 5.5$, $\Pi = 0.55$ for a flat plate, and $\delta(x)$ is the boundary layer thickness distribution. The corresponding Reynolds number distribution for length scale $L \equiv \delta(x)$ is,

$$Re_\delta = \frac{U_r \delta}{\nu} = 0.14(Re_x)^{6/7} \qquad (33)$$

where $U_r = U(x)$ is the reference free stream velocity distribution. Figure 9a shows the problem geometry and a 19 × 19 nodal nonuniform mesh with local wall region resolution. The inlet flow is the slug profile $U(x_o) = 1$; hence, $\omega(x_o) = 0$ and Ψ_o is proportional to y. The inlet conditions for k_o and ϵ_o can be determined from the second x-station solution using Cole's law skin fraction

$$C_f \equiv \frac{\tau_\omega}{\rho U_o^2/2} = 0.455\left[\ln(0.06\ Re_x)\right]^2 \qquad (34)$$

A vanishing normal outflow boundary condition is appropriate for all variables in $q = \{\omega, k, \epsilon; \Psi\}$. The entrainment (top) boundary conditions are vanishing normal derivative for k and ϵ, $\omega = 0$, and $\partial\Psi/\partial n = U_r$. Finally, if appropriate, the wall function boundary data are employed along a line in the vicinity $y^+ \approx 50$.

The TWS solution was initialized from Cole's law (Equation 32) for $Re_{xf} = 4 \times 10^8$, where $xf = 32.6$ ft. Figure 9b graphs the resultant boundary layer profile development on $0 \le x \le xf$. The CFD comparisons with Cole's law at station $x = 25$ ft, where $Re_x = 1 \times 10^8$, are drawn for vorticity and velocity in Figures 9c and d. The solid line is Cole's law (exact solution) and the symbols are the CFD solution. Agreement is very good on all bases, indicating CFD prediction accuracy for growth of a turbulent boundary layer. Figures 9e and f show the companion computed profiles for k and ϵ.

SUMMARY AND CONCLUSIONS

This paper has presented an overview of mathematical theory, closure modeling, and code validation issues of pertinence to room air motion CFD prediction. A series of critical benchmark problem predictions are

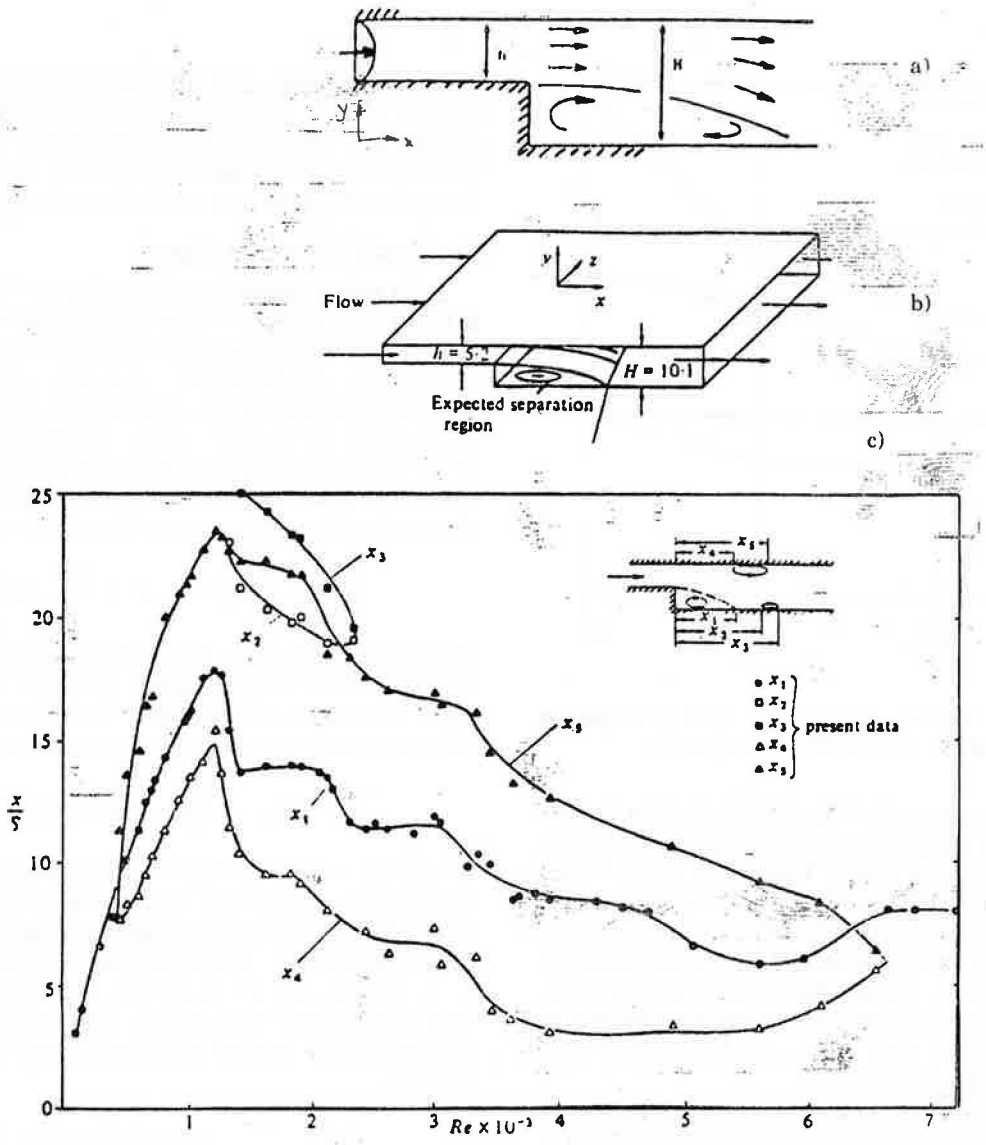

Figure 5 *Close-coupled step wall diffuser, a) two-dimensional, b) three-dimensional, c) experimental data of Armaly et al. (1983)*

A series of critical benchmark problem predictions are highlighted and discussed that serve assessment needs for code validation. Specific emphasis has been placed on identification of error mechanisms that lurk at every turn to pollute a CFD solution.

By and large, the correction of mathematically based discrete approximation errors lies strictly in the use of computational meshes with sufficient refinement to resolve local solution gradients. Without an adequate level of refinement, strictly numerical dissipation mechanisms become dominant, and totally pollute a coarse mesh CFD solution. Factually, if a coarse mesh solution appears smooth, one can be assured that numerical diffusion dominates the results. The indoor environmental analysis community must thus strive to become literate users of CFD methodology so that the inherent limitations are understood and fully appreciated. Further, the burden falls on CFD code designers to offer the full complement of validation test results to the prospective code user and/or buyer.

ACKNOWLEDGMENTS

This work was principally supported by ASHRAE under Research Project 464, entitled "Calculation of Room Air Motion." The authors wish to acknowledge the contributions of many graduate students in the University of Tennessee CFD graduate program, in particular Messrs. Wilbert Noronha, Jon Woods, Paul Williams, and Leif Wilkening. Computational resources were provided by the CFD Laboratory and the University of Tennessee Computer Center, both of which are gratefully acknowledged.

REFERENCES

AGARD. 1988. *Validation of computational fluid dynamics.* Symposium Papers and Roundtable Discussion, Report AGARD-CP-437, Vol. 1.

Armaly, B.F.; Durst, F.; Pereirz, J.C.F.; and Schonung, B. 1983. "Experimental and theoretical investigation of backward-facing step flow." *J. Fluid Mech.*, Vol. 127, pp. 473-496.

Baker, A.J. 1983. *Finite element computational fluid mechanics.* Washington, DC: Hemisphere.

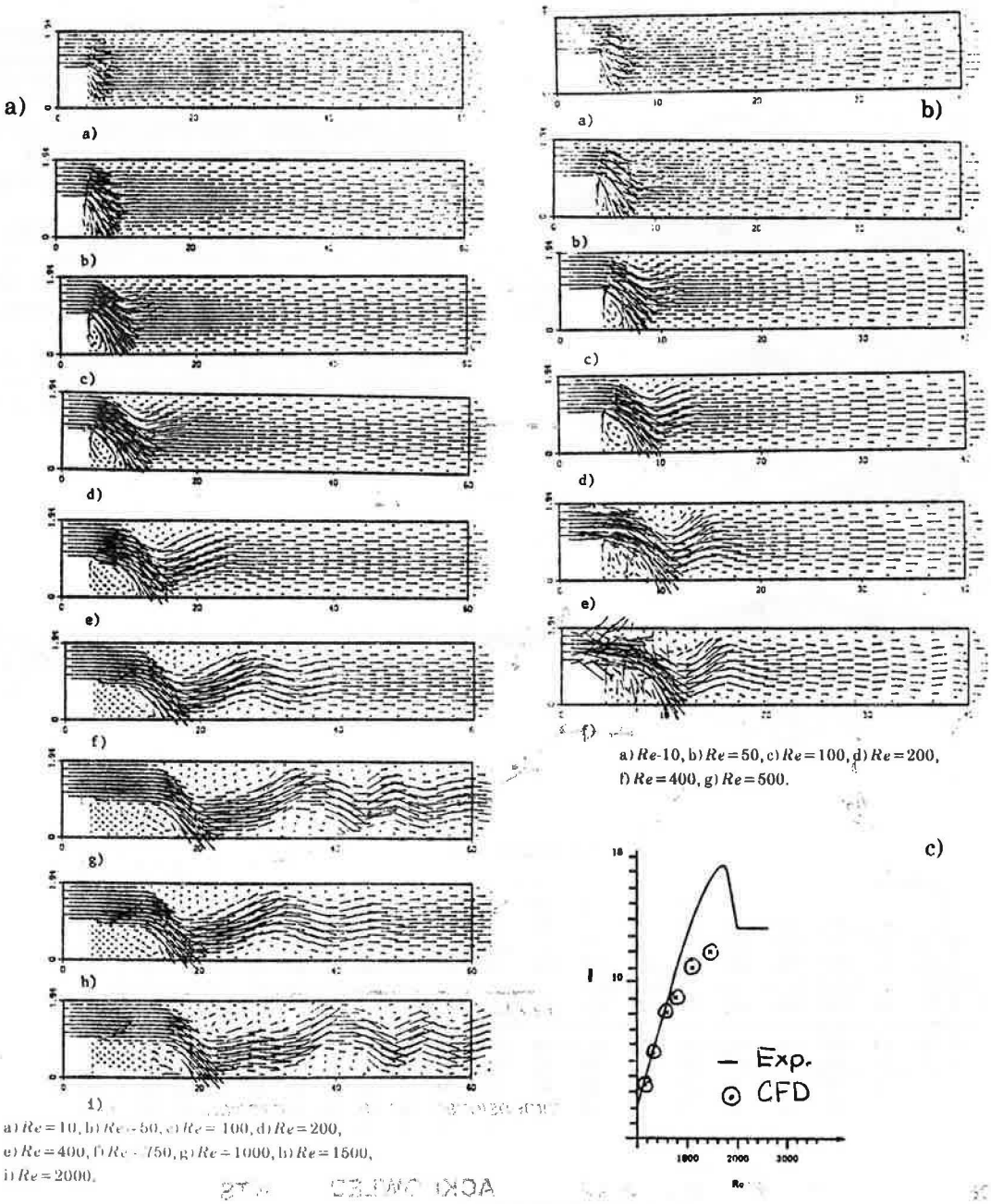

Figure 6 *Close-coupled step wall diffuser benchmark test, 10 ≤ Ref ≤ 2000, steady velocity fields; a) TWS $\omega - \Psi$ algorithm, $v_\omega = 0$; b) TWS u-v penalty algorithm, $v_u \geq 0$; c) primary recirculation region span comparison, from Noronha and Baker (1989)*

Baker, A.J., and Kim, J.W. 1987. "A Taylor weak statement for hyperbolic conservation laws." *Int. J. Num. Mtd. Fluids*, Vol. 7, pp. 489-520.

Baker, A.J., and Pepper, D.W. 1990. *Finite elements, 1-2-3*. New York: McGraw-Hill, to appear.

Bradley, R.G. 1988. "CFD validation philosophy." Paper 1 in Report AGARD-CP-437, Vol. 1.

Chorin, A.J. 1967. "A numerical method for solving incompressible viscous flow problems." *J. Comp. Phys.*, Vol. 2, pp. 12-26.

Engleman, M.S. 1984. *FIDAP, fluid dynamics analysis program, user/theoretical manual.* Control Data Report No. 84000 3650.

Haghighat, F.; Jiang, Z.; and Wang, J.C.Y. 1989. "Natural convection and air flow pattern in a partitioned room with turbulent flow." *ASHRAE Transactions*, Vol. 95, Part 2.

Kwak, D.; Chang, J.L.C.; Shanks, S.P.; and Chakravarthy, S.R. 1986. "A three-dimensional incompressible Navier-Stokes flow solver using primitive variables." *AIAA Journal*, Vol. 24, pp. 390-396.

Lam, C.K.G., and Bremhorst, K. 1981. "A modified form of the k-ε model for predicting wall turbulence." *ASME Transactions*, Vol. 103, pp. 456-460.

Murakami, S.; Kato, S.; and Suyama, Y. 1987. "Three dimensional numerical study of turbulent airflow in a ventilated room by means of a two-equation model." *ASHRAE Transactions*, Vol. 93, Part 2.

Noronha, W.P., and Baker, A.J. 1989. "A Taylor weak statement finite element algorithm for 2D incompressible Navier-Stokes equations." Tech. Paper AIAA-89-0659.
Noronha, W.P.; Baker, A.J.; and Williams, P.T. 1990. "A time-accurate unsteady incompressible Navier-Stokes CFD algorithm." Technical Paper AIAA-90-0238.
Patankar, S.V. 1980. *Numerical heat transfer and fluid flow.* Washington, DC: Hemisphere.
Patel, V.C.; Rodi, W.; and Scheuerer, G. 1985. "Turbulence models for near-wall and low Reynolds number flows: a review." *AIAA Journal,* Vol. 23, pp. 1308-1319.
Roach, P.J. 1972. *Computational fluid dynamics.* Albuquerque, NM: Hermosa.
Woods, J.B. 1989. "A workstation-based expert system environment for a CFD laboratory Navier-Stokes computer code." M.S. thesis, Dept. Engr. Science and Mechanics, University of Tennessee.

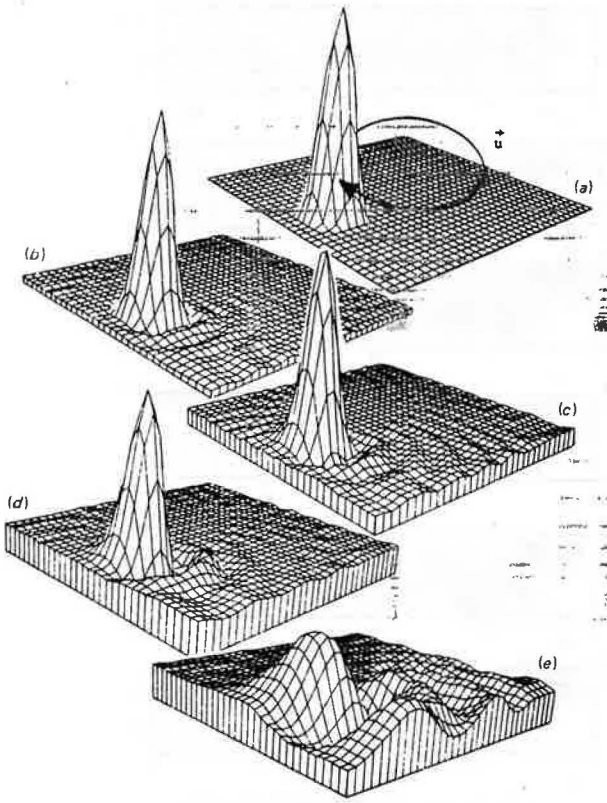

Figure 7 *The rotating cone benchmark problem; a) initial condition; b) FE, k = 2, C = 0.25; c) FE, k = 2, C = 0.5; k = 1, C = 0.25; d) FE, k = 1; C = 0.5; e) FD/CN, C = 0.25*

a)

Finite element, $k = 1$

															1	1	2	2	3	1
																				3
		Source				−1				1	1	2	3	5	5	6	8	9	9	10
							4	6	9	12	14	16	18	20	21	22	24	25	25	26
			2	12	21	28	35	38	41	44	45	46	47	48	48	48	49	49	49	49
	0	8	50	93	100	97	96	93	90	88	86	83	81	79	77	75	74	72	71	69
	0	16	92	159	156	142	132	123	116	110	105	100	97	94	90	87	85	82	80	78
U →	0	25	98	162	166	145	137	129	121	115	109	105	100	97	93	90	88	85	83	81
	−2	10	94	169	164	148	138	129	122	116	111	106	101	98	95	91	89	86	83	81
	−1	4	50	97	103	101	98	95	93	90	88	86	83	81	80	77	76	74	73	71
			2	10	19	26	31	35	38	41	43	44	45	46	47	47	48	48	48	48
				−2	−2	−1	1	3	6	9	11	14	15	17	19	20	22	23	24	25
											1	2	2	4	5	5	7	8	8	9
																	1	1	2	2
																				1

Gaussian

Finite element, $k = 2$

b)

Finite element, $k = 1$

															1	1		1
	Source						1	1	1	2	2	3	3	3	3	3		2
				3	4	5	7	8	8	8	8	8	8	8	8	8		5
	2	11	19	23	23	23	21	20	19	18	17	16	16	15	14	14		11
	7	42	74	73	55	48	43	35	32	29	27	25	23	22	20	19	18	17
	15	80	122	105	70	59	51	40	36	33	30	28	26	24	22	21	20	20
U →	25	93	137	113	79	62	52	44	39	35	31	28	26	24	22	21	20	Gaussian
	12	81	131	110	72	61	54	43	38	35	32	29	27	25	23	22	21	20
	4	43	78	76	57	50	45	36	33	31	28	26	24	23	21	20	19	17
	−1	2	12	20	25	25	24	22	21	20	19	18	17	16	16	15	14	11
					4	5	6	8	8	8	9	9	9	9	9	9	8	5
								1	1	2	2	3	3	3	3	3	4	2
															1	1	1	1

Finite element, $k = 2$

Figure 8 *Finite element Galerkin algorithm computed steady-state pollutant distributions comparison to Gaussian plume, linear and quadratic basis; a) two-dimensional, b) three-dimensional, from Baker (1983, p. 214)*

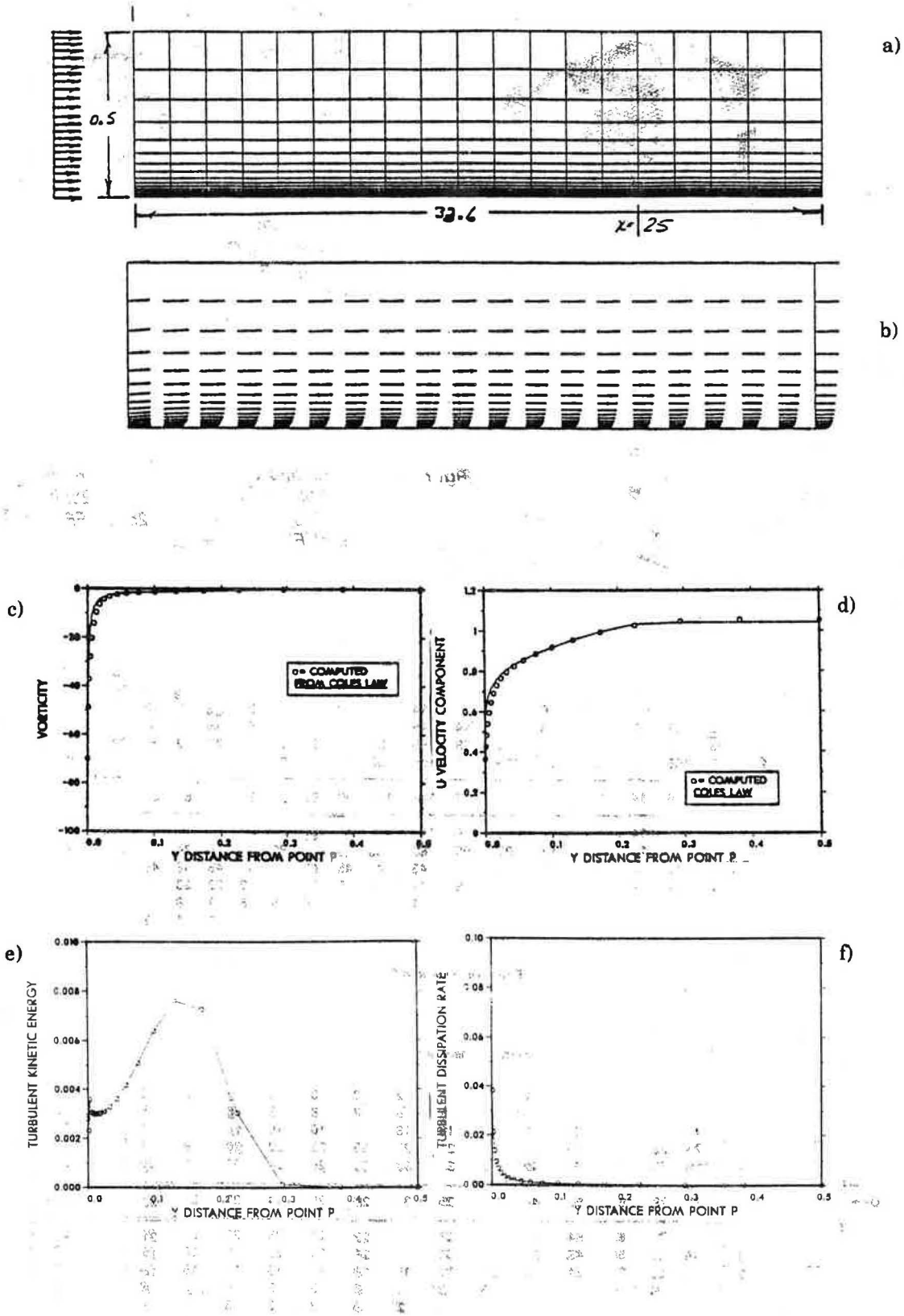

Figure 9 *Developing turbulent flow over a flat plate, wall functions, $Re_L = 4 \times 10^6$; a) mesh; b) velocity vector field at x = 25 ft, $Re_x = 10^6$; c) vorticity; d) U velocity; e) turbulent kinetic energy; f) dissipation function*